Water behavior, equilibrium, and migration of a biomaterial made of pure mycelium

Brahim Mazian, Hasna Nait M'barek, Giana Almeida, Pedro Augusto, Patrick Perré

Water behavior, equilibrium and migration of a biomaterial made of pure mycelium

Brahim Mazian[1], Hasna Nait M'barek[1], Giana Almeida[2], Pedro Augusto[1], Patrick Perré[1,3]

[1]Université Paris-Saclay, CentraleSupélec, Laboratoire de Génie des Procédés et Matériaux, Centre Européen de Biotechnologie et de Bioéconomie (CEBB), 3 rue des Rouges Terres 51110 Pomacle, France.

[2]Université Paris-Saclay, INRAE, AgroParisTech, UMR SayFood, 91120, Palaiseau, France.

[3]Université Paris-Saclay, CentraleSupélec, Laboratoire de Génie des Procédés et Matériaux, 3 rue Joliot Curie, 91190 Gif-sur-Yvette, France.

Abstract

Mycelium materials are an emerging class of natural, inexpensive, and environmentally sustainable materials. They are promising alternatives to petroleum-based polymeric ones, and they can also be used as substitutes for animal-based leather. This work investigates the water relation properties (equilibrium and transfer) of pure mycelium materials produced using *Ganoderma lucidum* fungal species in liquid-state fermentation. The dynamic gravimetric method was used to determine sorption isotherms at four temperatures (20°C, 30°C, 40°C and 50 °C) over a water activity (a_w) range of 0 to 0.9. This material is highly hygroscopic and depicts a huge condensation phase at high water activity, with an equilibrium moisture content of 53% at 20 °C and 90% RH. Among the eight sorption models tested, the GAB model gives good results and was further used to analyze data. Thermodynamic properties (net isosteric heat of sorption, sorption entropy change, and the isokinetic temperature) were determined from the sorption isotherms to represent better the energy related to the sorption processes. Finally, the transient stages of sorption measurement were analyzed to extract mass transfer properties. Consistently with the morphology of this material, a dual-scale effect is evidenced, which turns into a representation by two independent parameters: the macroscopic and microscopic mass diffusivity values.

Keywords: biomaterial; biobased materials; leather-like; fungi; water sorption; mass transfer

1. Introduction

Fungal mycelium materials are among the most emerging classes at the crossroads of biotechnology and material engineering sciences [1–3]. Humans have long used fungi to produce food (e.g., cheese, bread, and beer) or in medical biotechnology (antibiotics and antivirals [4]). Recently, fungi were also suggested as a substitute resource to develop new environmentally friendly substitutes for leather [5–7]. In fact, recent developments in fungal biotechnology and their integration into materials science are opening up new perspectives in different applications, such as the fashion and textile fields [8].

The use of natural mechanisms of biological development has a remarkable combination of complementary functional properties for bio-leathers production. These bio-leathers, produced by natural mechanisms, have the potential to contribute to the new economy by substituting natural leather sourced from animals [7]. The use of bio-leather from fungal mycelium materials can reduce unnecessary slaughter to obtain animal leather.

Mycelium mat is a vegetative part of fungi. It is a dense network of thin strands called hyphae, which is the basic developmental unit of fungi. The main constituent present in the hypha wall is chitin, which ensures its stiffness and strength [9]. Mycelium material mats could be grown using solid-state fermentation or liquid-state fermentation [7]. In both methods, fungi require direct contact with their nutrient source. In solid-state fermentation, the growth can be performed on a solid substrate [3, 10]. The hyphae can interlock the substrate within its network and outward growth away from the substrate into the air. This requires specific conditions of nutrients, temperature, oxygen, CO_2 partial pressure, light, and mostly a high relative humidity (40–99%), to be tightly controlled using incubation chambers [2]. These conditions prevent the development of fruiting bodies from the mycelium, as they are promoted by low temperatures and CO_2 concentrations. Greetham et al. 2015 associate the outward growth of the mycelium in the substrate to the carbon dioxide gradient caused by cellular respiration. The accumulation of CO_2 inside the substrate naturally generates a gradient along which the mycelium will grow outwards the outside to a more O_2-rich environment. Liquid-state fermentation is the most used method to produce pure mycelium materials [12, 13]. This method involves placing a sterilized nutrient medium in a closed vessel, inoculating the fungal spores, and letting the mixture undisturbed to allow the fungus to form a mat of hyphae at the surface of the liquid. Once the obtained mycelium mat has dried, it looks like leather.

Although the interest in mycelium materials is increasing, their properties still need to be better understood in special the interaction of pure mycelium material with water (behavior,

equilibrium and transfer). Water transfer (absorption, desorption and diffusivity) occurs during the use of materials, as a response to the change of environmental conditions, and dual-scale mechanisms and/or molecular relaxation are often observed for the product of biological origin [14,15].Therefore, the best knowledge of the equilibrium moisture content and transfer properties of mycelium mat with its surrounding environment leads to a better understating of the product behavior during storage and usage conditions.

The aim of this study is to investigate the water behavior, both equilibrium and dynamic, of a fungal mycelium mat. To achieve this, desorption and adsorption isotherms of fungal mycelium mats were experimentally determined using a dynamic vapor sorption method at temperatures ranging from 20°C to 50°C and humidity levels ranging from 0 to 90%. Mathematical modeling was then performed on the experimental equilibrium data to select the best-fitting equation for the considered operating conditions. Using the best-fit sorption model, different thermodynamic functions were determined, including the isosteric heat of sorption and sorption differential entropy at different moisture contents. In addition, the diffusion mechanisms were studied by determining the mass diffusivity using inverse analysis from the experimental moisture content evolution. A comprehensive macroscopic model of coupled heat and mass transfer was used, and a dual-scale model, based on the concept of distributed microstructure models with coupled heat and mass transfer at both scales, was used to simulate the experiments.

2. Materials and Methods

2.1.Sample preparation

Ganoderma lucidum (BRFM 953) stock culture was procured from the *Centre International de Ressources Microbiennes - Champignons Filamenteux* (CIRM-CF), INRAE Marseille, France. It was conserved in semi-aerated slots of solid culture at 4 °C, cultured in solid plates of MA2 medium (per 1 L MilliQ-grade water: malt extract 30 g, soya peptone 3 g; pH 5.6) and maintained regularly. For all experiments, growth was conducted at 25 °C in absolute darkness to avoid natural fructification of the mycelium under the light. *Ganoderma lucidum* is of interest due to its ability to produce a dense mycelial network with high mechanical properties [6], making it a suitable material for producing eco-friendly leather-like products. Pure mycelium mats were produced in liquid fermentation using MA2 nutritive medium. 300 mL flasks containing 100 mL autoclaved MA2 were inoculated using one-week-old actively growing hyphae and were statically incubated at 25 °C for four (4) weeks [16] . A dense hyphal network started developing on the surface, growing over time, and forming a well-nested and consistent mat. At the end of the growth period, media were carefully filtered to retrieve the pure mycelium materials (Figure 1b), which were rinsed thrice with MilliQ-grade water, dried on filter paper, and used for characterization.

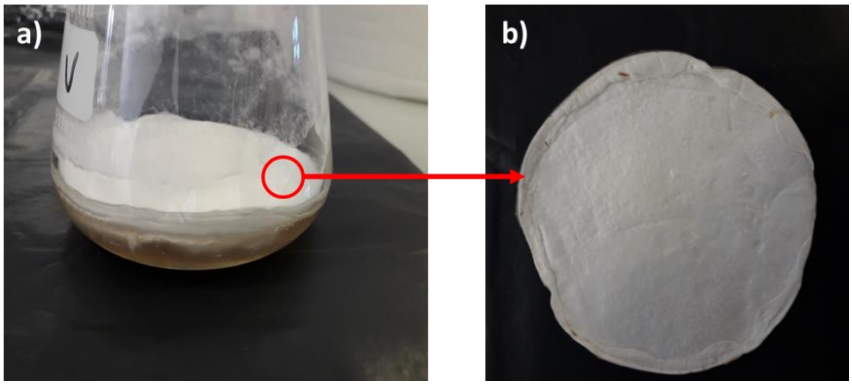

Figure 1: Production of Ganoderma lucidum mats. a) spongy hyphal network formed in the surface of the growth medium after four weeks, b) final mycelium materials.

2.2.Microscopic observations

Microscopic images of the samples were obtained using an environmental scanning electron microscope (ESEM, Quanta 200, FEI Company). Images were taken in Low Vac mode, at 107 Pa, voltage 12 kV, with a beam spot size of 3.5 and a working distance of approximately 8 mm.

The Low Vac mode allows samples to be imaged without any coating even though they are not electrically conductive. Image were grabbed at low voltage to limit the beam penetration and the working distance is a compromise between the detector signal and the degradation of the electron beam in the chamber, which is not in a secondary vacuum. Samples for imaging were extracted from various spots across the disc at two growth intervals: three and four weeks. Once chosen, these samples were affixed to a carbon conductive double-sided adhesive disc without additional preparations. The width distribution of mycelium was determined by image analysis using ImageJ, where the width of each mycelium strand was automatically measured using the DiameterJ plugin.

2.3.Moisture sorption isotherms

The sorption isotherms (adsorption and desorption) were determined using dynamic vapor sorption (DVS) equipment (IGASorp-HT system, from Hiden Isochema Co, Warrington, England). This instrument is composed of a climatic chamber equipped with an ultra-sensitive microbalance (0.1µg in resolution) which allows monitoring the mass variation as a function of the ambient temperature and relative humidity. A mix of a separate wet stream and dry nitrogen stream, controlled by two different mass flow controllers is used to set the desired RH value. A Rotronic humidity probe (accuracy of ± 1 % between 0-90 %RH and ± 2 % between 90-95 %RH) is used to control RH in the chamber (control stability ± 0.1 %RH). In this study, nitrogen was selected as the carrier gas with a 250 mL/min flow. The temperature is measured by PT100 platinum probe (accuracy of ± 0.1 °C) and controlled at ± 0.05 °C.

Equilibrium sorption isotherms, for adsorption and desorption, were carried out at four temperatures (20 °C, 30 °C, 40 °C and 50 °C) for selected water activities a_w in the range 0-0.90 with an increment of 0.15. The measurement procedure is as follows: the dry weight of the sample is obtained in the first step. Then, the desired humidity level is set, and the changing weight signal is recorded at every 10 seconds. Equilibrium in a moisture sorption experiment is defined as the point where the moisture content stabilizes or reaches a steady state. In this study, it was determined using a criterion of 99% of the predicted equilibrium mass uptake, estimated by a simple asymptotic rise model for forward prediction. Once equilibrium was reached, the next humidity step was initiated. Equilibrium moisture content is defined as the ratio of water contained in the sample at equilibrium (total weight – dry weight) over the dry weight.

3. Water- product relations

3.1.Sorption isotherms

In this study, eight models have been evaluated to fit the sorption isotherms of mycelium mats (Table 1). The suggested models were selected based on their applicability and popularity in the literature for describing the moisture sorption behavior of biobased materials. Some models are developed with a theoretical basis, such as GAB, BET and Langmuir [17–19] others are based on semi-theoretical and empirical equations [20–23]. The model parameters were fitted to the experimental data using the nonlinear regression analysis of the Origin software. The goodness of fit of different models between the experimental and predicted equilibrium moisture content was evaluated with the correlation coefficient (R^2)(Eq. (1)), the root mean square error (RMSE) (Eq. (2)) and sum squared errors (SSE) (Eq. (3)).

$$R^2 = \sqrt{\frac{\sum_{i=1}^{N}\left(Xeq_{i,pre} - \overline{Xeq}_{i,exp}\right)^2}{\sum_{i=1}^{N}\left(Xeq_{i,exp} - \overline{Xeq}_{i,exp}\right)^2}} \quad \text{Eq. (1)}$$

$$RMSE = \left[\frac{1}{N}\sum_{i=1}^{N}\left(Xeq_{i,exp,i} - Xeq_{i,pre}\right)^2\right]^{1/2} \quad \text{Eq. (2)}$$

$$SEE = \sqrt{\frac{\sum_{i=1}^{N}\left(Xeq_{i,exp} - Xeq_{i,pre}\right)^2}{d_f}} \quad \text{Eq. (3)}$$

Where N is the number of data points; $Xeq_{i,exp}$ is the experimental moisture content (%d.b); $Xeq_{i,pre}$ is the predicted moisture content (%d.b).

Table 1: The different models fitted to represent the experimental data of moisture sorption isotherm of mycelium mat

	Model	Mathematical equation	Parameters
Theoretical basis	GAB [19]	$Xe = \left(\frac{X_m.C.k.a_w}{(1-k.a_w)(1-Ka_w+C.k.a_w)} \right)$	$X_m,\ C,\ k$
	BET [17]	$Xe = \left(\frac{X_m.C.a_w}{(1-a_w).(1-a_w+C.a_w)} \right)$	$X_m,\ C$
Semi-theoretical / empirical equations	Langmuir [18]	$X_e = \frac{1}{A+B.x^{C-1}}$	$A,\ B,\ C$
	Oswin [23]	$X_e = A.\left(\frac{a_w}{(1-a_w)} \right)^B$	$A,\ B$
	Halsey [24]	$X_e = \left(\frac{-A}{ln(a_w)} \right)^{1/B}$	$A,\ B$
	Peleg[25]	$X_e = A.(a_w)^B + C.(a_w)^D$	$A,\ B,\ C,\ D$
	Enderby[21]	$X_e = \left[\frac{A}{1-Ba_w} + \frac{C}{1-Da_w} \right] a_w$	$A,\ B,\ C,\ D$
	Caurie [26]	$X_e = \exp(A+B.a_w)$	$A,\ B$

3.2.Net isosteric heat of sorption (q_{st})

The net isosteric heat of sorption q_{st}, also named differential heat of sorption, quantifies the water affinity energy with the absorbent, as compared to liquid water. It is defined as the difference between the total heat required to remove water from the product (Q_{st}) and the heat required to vaporize pure liquid water (ΔH_{vap}), at given conditions:

$$q_{st} = Q_{st} - \Delta H_{vap} \qquad \text{Eq. (4)}$$

The isosteric net heat of sorption can be derived from the best-fitting sorption isotherms model at various temperatures using the Clausius-Clapeyron equation [27, 28]:

$$\frac{d(\ln(a_w))}{d\left(\frac{1}{T}\right)} = -\frac{q_{st}}{R} \quad \text{Eq. (5)}$$

Where a_w is water activity, T is the selected temperature (K), R is the universal gas constant (8.314 J.mol^{-1} K^{-1}) and q_{st} is the net isosteric heat of sorption (kJ.mol^{-1}).

Based on Eq. (5), the isosteric net heat of sorption is calculated from the slope of $\ln(a_w)$ versus 1/T at a fixed value of equilibrium moisture content. This procedure was repeated for different moisture contents. The slopes in Equation (5) were determined using the four temperature values.

3.3.Sorption differential entropy (ΔS)

Entropy is a thermodynamics state variable that characterizes the disorder, randomness, or uncertainty degree in the water-sorbent relationship. Sorption entropy is useful to explain many processes, such as dissolution, crystallization and swelling, which usually occur during the sorption of water content by materials [29, 30]. The differential entropy or sorption differential entropy (ΔS) of materials is associated with the number of sorption sites available at a specific energy level. It corresponds to water molecules' forces (attraction or repulsion) to the sample.

The sorption entropy is obtained using the Gibbs-Helmholtz relation (Eq.6) :

$$\Delta S = \frac{q_{st} - \Delta G_b}{T} \quad \text{Eq. (6)}$$

ΔG is the Gibbs free energy. It is defined as :

$$\Delta G = -RT\ln(a_w) \quad \text{Eq. (7)}$$

By combining equation (6) and (7), the net isosteric entropy at each moisture can be presented as follows:

$$\ln(a_w) = -\frac{q_{st}}{RT} + \frac{\Delta S}{R} \quad \text{Eq. (8)}$$

The intercept (ΔS/R) of the curve representing $\ln(a_w)$ as a function of 1/T is used to determine the sorption of a given moisture entropy.

3.4.Enthalpy-entropy compensation theory

The enthalpy–entropy compensation, or thermodynamic compensation theory is commonly used to study different physical and chemical processes, including the relationship of

biomaterials with the water [31]. It suggests a linear relationship between the net isosteric heat of sorption and sorption differential entropy for determining moisture content [32]. The linear relation is presented in Eq. (9).

$$q_{st} = T_{\beta}\Delta S + \Delta G_b \quad \text{Eq. (9)}$$

T_{β} corresponds to the isokinetic temperature, representing the temperature at which all series reactions proceed at the same rate. ΔG_{β}, the free energy at isokinetic temperature, represents whether the water sorption process is spontaneous ($\Delta G_{\beta} < 0$) or non-spontaneous ($\Delta G_{\beta} > 0$). In order to test the validity of the compensation theory, the isokinetic temperature T_{β} must be compared with the harmonic mean temperature T_{hm} (Eq. (10)).

$$T_{hm} = \frac{n}{\sum_{i=1}^{n}(1/T_i)} \quad \text{Eq. (10)}$$

Leffler and Grunwald, 2013 consider the process is enthalpy-driven if ($T_{\beta} > T_{hm}$), whereas the process is entropy-controlled if ($T_{\beta} < T_{hm}$).

3.5.Dual-scale model of moisture transfer

During the sorption tests, the DVS equipment records all parameters versus time, namely the actual chamber conditions (temperature and relative humidity) and the sample mass. The acquisition frequency is high enough (6 points per minute) to accurately define the transient stages. In addition to the equilibrium values, the sole information used to define the sorption isotherms, an inverse analysis of these transient phases was performed to extract relevant information on water transfer. The procedure minimizes the objective function using a comprehensive set of macroscopic equations of coupled heat and mass transfer [33]. However, for this kind of porous morphology (solid inclusions arranged in a strongly connected gaseous phase – see the morphological results as follows), non-Fickian behavior is likely to occur due to the dual-scale effect, and the classical macroscopic equation is not relevant anymore [15, 33].

To address this issue, the extended macroscopic formulation is presented in Perré. 2019 was used. The dual-scale effect due to the characteristic diffusion time in the solid inclusions themselves is accounted in for the macroscopic formulation by the so-called memory function.

The memory function is defined by an ideal (virtual) test in which the storage phase (the inclusions) is submitted to a sudden change in relative humidity from initial relative humidity (RH_{ini}) to final relative humidity (RH_{fin}).

$$X(t) - X_{ini} = \Delta X_{eq} \varphi(t) \qquad \text{Eq. (11)}$$

In this equation, X_{ini} is the equilibrium moisture content at the initial RH value, ΔX_{eq} is the change of equilibrium moisture content from RH_{ini} to RH_{fin} and φ is the memory function, which represents the dimensionless evolution in time of the average moisture content of the inclusions. This is a monotonic function that tends to unity as t tends to infinity.

In a real test, the RH value surrounding the inclusion varies over time and a convolution product is required to account for this time dependence:

$$X(t) - X_{ini} = \int_0^t \varphi(t-\tau) \frac{\partial X_{eq}}{\partial \tau} d\tau \qquad \text{Eq. (12)}$$

When representing the memory function as a series of exponential functions, the convolution product can be simply treated as internal variables. Two exponential functions are a good compromise to represent the diffusion in simple geometry inclusions (cylinders here). The exponential values proposed in Perré. 2019 for cylindrical inclusions were considered here (Table 2). Note that the characteristic times are tied to both the microscopic bound water diffusivity D and the dimension of the inclusion (radius a for a cylinder).

Table 2: Parameter values to approach diffusion in a cylindrical inclusion with two exponential functions (according to Perré, 2019).

Parameters	Values
α_1	0.72546
$\tau_1 / (a^2 / D)$	0.16732
α_2	0.26074
$\tau_2 / (a^2 / D)$	0.01208

To account for the memory effect, X should be used for mass balance while all driving forces involved in convective or diffusive fluxes should be tied to X_{eq} to consider the right water activity a_w. The extended mass balance equation therefore reads [34]:

$$\rho_0 \frac{\partial X}{\partial t} + \nabla \cdot \left(\mathbf{q}_m (X_{eq}) \right) = \nabla \cdot \left(\mathbf{j}_m (X_{eq}) \right) \quad \text{Eq. (13)}$$

Where X and X_{eq} are linked by a convolution product:

$$\frac{\partial X}{\partial t} = \frac{\partial}{\partial t} \left(\int_0^t \varphi(t-\tau) \frac{\partial X_{eq}}{\partial \tau} d\tau \right) \quad \text{Eq. (14)}$$

The computational model used in the inverse procedure, *TransPore*, considers three balance equations allowing three variables to be predicted in time and space, for example: temperature, moisture content and pressure [14]. The third equation is solved but is not necessary here because the thinness of the mycelium materials, combined with their high permeability, ensures that the pressure remains at atmospheric pressure through the thickness.

On the contrary, the heat and mass coupling is important, either at the interface or inside the product [35] and must be considered. Removing the unnecessary terms related to liquid water, not involved in the sorption test, the enthalpy balance read as:

$$\begin{aligned} &\frac{\partial}{\partial t} \left(\varepsilon_g (\rho_v h_v + \rho_a h_a) + \overline{\rho_b h_b} + \varepsilon_s \rho_s h_s \right) \\ &+ \nabla \cdot \left((\rho_w h_v + \rho_a h_a) \overline{\mathbf{v}}_g \right) = \nabla \cdot \left(\lambda_{eff} \nabla T + (h_v - h_a) \rho_g \mathbf{f} \mathbf{D}_v \nabla \omega_{v,eq} \right) \end{aligned} \quad \text{Eq. (15)}$$

The external heat and mass transfer coefficient, respectively h_h and h_m, are involved in the boundary conditions:

$$\begin{aligned} j_h \big|_{x=0^+} &= h_h \left(T \big|_{x=0} - T_\infty \right) \\ j_v \big|_{x=0^+} &= h_m \, c \, M_v \ln \left(\frac{1 - x_\infty}{1 - x_v \big|_{x=0}} \right) \\ P_g \big|_{x=0^+} &= P_{atm} \end{aligned} \quad \text{Eq. (16)}$$

4. Results and discussion

4.1.Structure and morphology of the obtained material

Ganoderma lucidum is a polypore known for its versatility, invasive growth on wood benches and the health-protective properties of its metabolites [36]. Although it has a long biological

cycle, which takes from eight months to a year, the early mono and dikaryotic mycelial stages are fast occurring when the right environmental conditions are set. Mycelial colonization can thus happen in a few weeks [36]. During early stages of growth, *Ganoderma lucidum* produces thick and septate generative hyphae that thrive on substrate and fully settle on. Afterwards, skeletal filaments are produced, as a way to strengthen the network [16, 37]. They are long, non-septate, unbranched and continuously oriented along a specific direction (Figure 2.a). In ESEM micrographs, generative hyphae (tube-like) have a characteristic width of 5-35 µm and the skeletal ones (thread-like) between 0.5-5 µm (Figure 2.b). These observations are supported by different findings [16]. After four weeks of growth, hyphae start to fuse and interconnect by anastomosis that shape the mat into a structurally-porous material with intersectional nodes (Figures2.c and d). The trimitic hyphal composition is well-confirmed in *Ganoderma lucidum* fungus with the presence of three mycelial structures. This being said, it is responsible for the tough, leathery, and woody fruiting bodies that *Ganoderma lucidum* can produce, and with no doubt, is correlating with cell-wall composition and hydrophilicity.

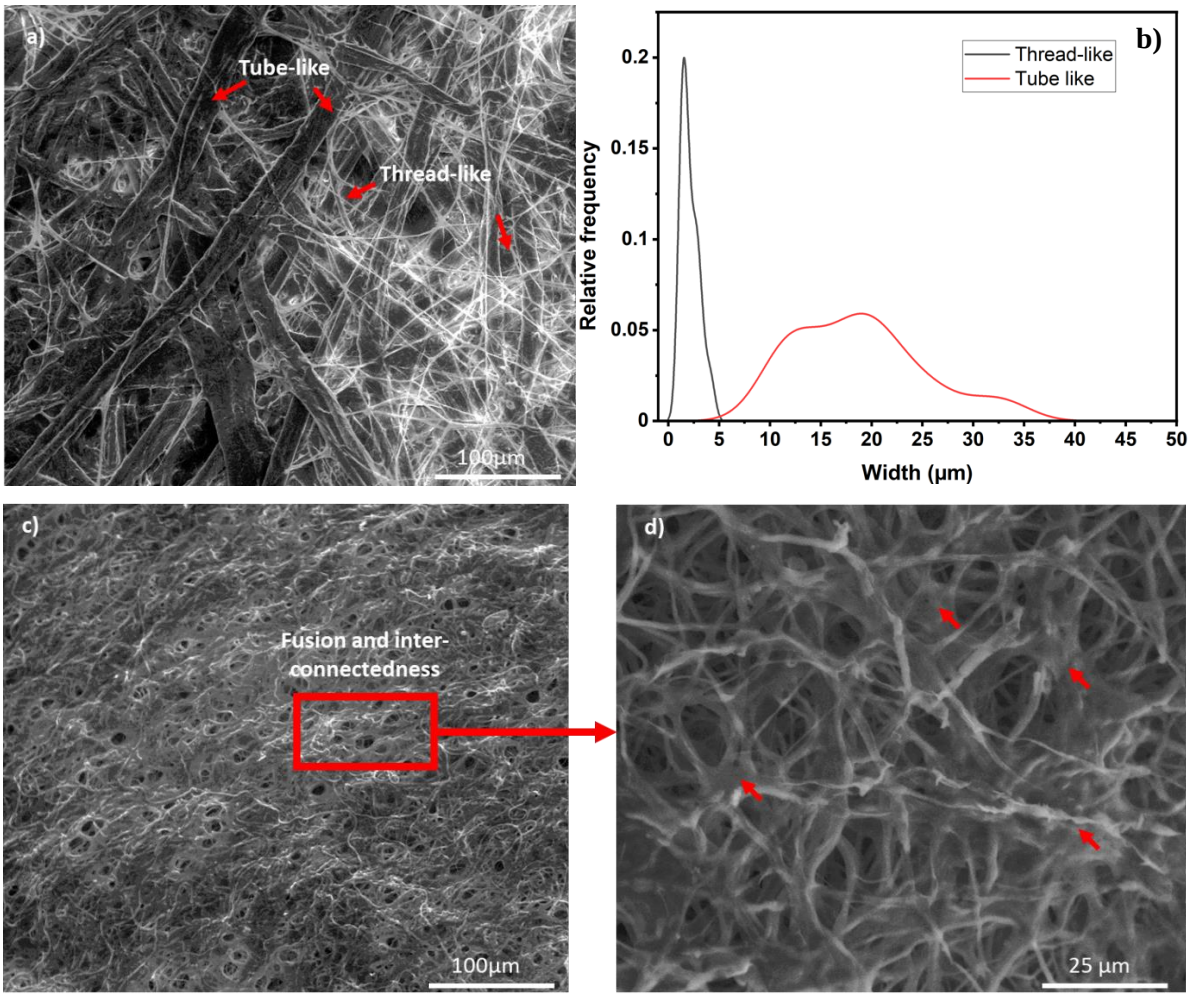

Figure 2: a) ESEM micrograph of a three-week Ganoderma lucidum mycelium mat presenting generative (tube-like) and skeletal (thread-like) hyphae (magnification X500); b) Size distribution of both hyphae types using ImageJ; c and d) Porous material after fours week of growth. Red arrows: fusion and inter-connectedness of mycelium structures (c :magnification X600; d: X2400 magnifications).

4.2.Sorption isotherms

Figure 3 displays the experimental results obtained for the equilibrium moisture content as a function of water activity, for adsorption and desorption, at four temperatures (20, 30, 40, and 50 °C). The equilibrium moisture content is presented on a dry basis (kg water per kg dry material). The shape of the isothermal sorption curve indicates how water is bound to the material. According to the classification developed by Brunauer et al. [17], the sorption isotherm of the mycelium mat presents a sigmoid shape of type II behavior. At low a_w values, the bound water is proportional to the water activity, which is explained by a monolayer of water molecules. At a water activity of around 0.15, the slope decreases, which is characteristic of a multilayer absorption. Finally, a large amount of moisture is adsorbed at higher water activity values, which is typical of capillary condensation in micropores. Such behavior is not unique to mycelium mats but is also evident in hydrophilic materials like bovine leather, cassava flour, and biomass [38–42]. For instance, the bound water content of mycelium mat resembles that of some leathers, particularly in their hygroscopic nature: At 25°C, mycelium mats' equilibrium moisture content increases from 5% (a_w = 0.15) to 53% (a_w = 0.90), similarly to bovine leather which rises from about 13% to 50% across the same a_w range [40].

As expected, the equilibrium moisture values decrease with increasing temperature at a given water activity. At a water activity of 0.9, the equilibrium moisture decreases from 53% to 28% when temperature increase from 20°C to 50°C. This is explained by the thermal agitation: at higher temperature, the water molecules easily detach from their binding sites.

Another behavior that can be observed during the adsorption and desorption processes is the hysteresis of sorption (Figure 4). This latter is defined as the difference between desorption and adsorption of equilibrium moisture content values at a given water activity. The sorption hysteresis is evident at 20°C, mainly at low water activity. However, there is a significant decrease in hysteresis magnitude with increasing water activity. The hysteresis phenomenon could be explained by structural and conformational rearrangements of macromolecules, or even of the mycelium mat in the domain of condensation, as observed for jersey and yarns made

of cotton [43]. At high moisture content, the molecular structure of the mycelium mat is filled up with adsorbed water. Consequently, when the water moves out from the capillaries of the mycelium mat, during the desorption process, the narrow ends of surface pores could trap and hold water internally, below the water activity where the water must be released.

It can also be seen in Figure 4 that increasing temperature leads to a decrease in the hysteresis magnitude. This perhaps could be related to the expansion of elasticity of capillary walls at higher temperatures, and greater capacity of forming hydrogen bonds between dry matter and moisture present in the mycelium mat [44].

Building upon these insights, the properties of mycelium mats bear similarities to those observed in certain traditional materials, such as cotton-based materials and leather [40, 43]. The remarkable ability of these materials to retain and regulate moisture has contributed significantly to their widespread use in various applications, including clothing, footwear, and protective gear. Given the analogous behaviours of mycelium mats in moisture regulation, they emerge as a promising and eco-friendly alternative to leather in these applications.

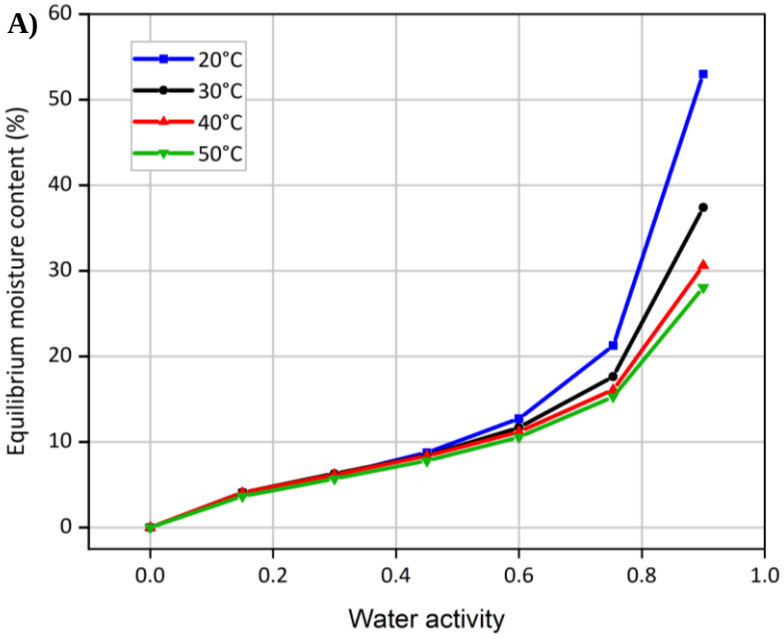

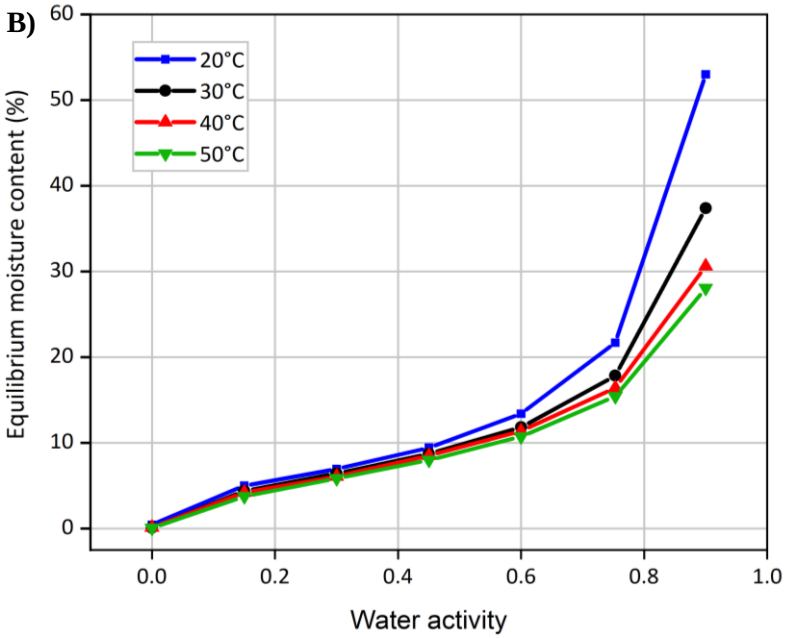

Figure 3. Impact of temperature on the equilibrium moisture content of mycelium mat A) adsorption isotherm B) desorption isotherm

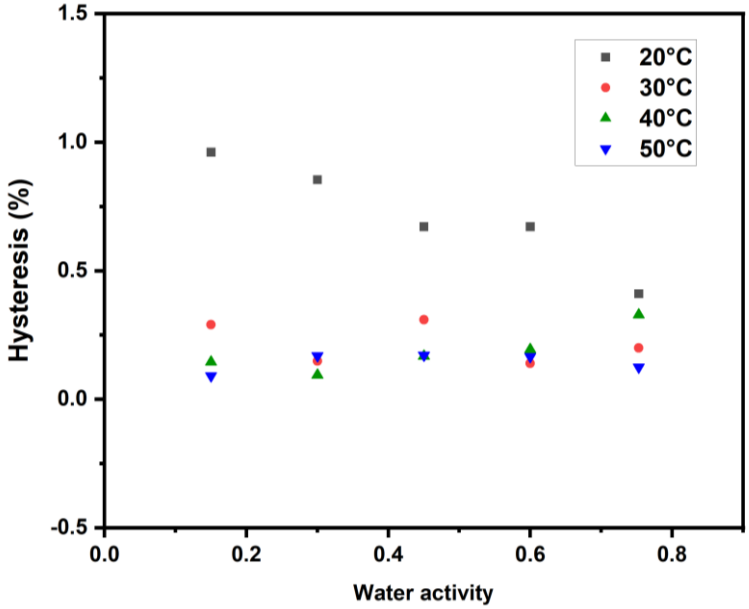

Figure 4. Hysteresis values (difference moisture content between desorption and adsorption isotherm at the same water activity)

4.3.Modelling of sorption isotherm

The sorption isotherm for the mycelium mat at four different temperatures were analyzed by using eight well-known isotherm models. The model parameters and their statistical calculations (R^2, RMSE, SSE) for sorption isotherms are given in supplementary material (Table 1S). The suggested model can be considered acceptable for higher R^2 values and lower

values of RMSE and SSE (tending to 0). A zero value of RMSE and SSE means that the model is a perfect fit of the available experimental points.

The results reveals that the Enderby, GAB, Halsey, Langmuir, and Peleg models can accurately represent the experimental data. However, the acceptability of a model is not solely based on its ability to fit observed data; it also requires a physico-chemical basis to extract thermodynamic properties. In this regard, the GAB model not only represents experimental data with acceptable precision (Figure 5 and Table 3), but also has a sound theoretical basis. It is a refinement of the BET and Langmuir physical adsorption theories and allows for a small error to be obtained with only three independent parameters. Moreover, the GAB model permits calculation of the monolayer moisture content (X_m), which indicates the amount of moisture adsorbed by a single layer to binding sites in the material. The X_m values are crucial because they represent the ideal moisture content to be obtained to guarantee the product stability, both in the drying processes and in the storage and application of the material. The obtained X_m in this study ranges between 5.0 – 5.5% (kg water/100 kg dry matter) for adsorption and desorption. By looking at the fitted values of the GAB model in sorption, some temperature trends are discernible:

- X_m, representing the monolayer moisture content, seems to exhibit a linear decrease with temperature. This suggests a gradual decrease in sorbate affinity with temperature due to thermal agitation,
- k displays a declining trend with increasing temperature. As the temperature rises, the sorption process for additional layers of moisture molecules appears to be less energetically favorable, resulting in lower values of k
- C exhibits a plateau or saturation effect at higher temperatures, indicating an upper limit to the influence of temperature. Beyond this point, further increase in temperature does not significantly impact this constant. This could indicate a transition in the multilayer sorption mechanism.

All further analyses of the sorption isotherms will be derived from the fitted GAB model.

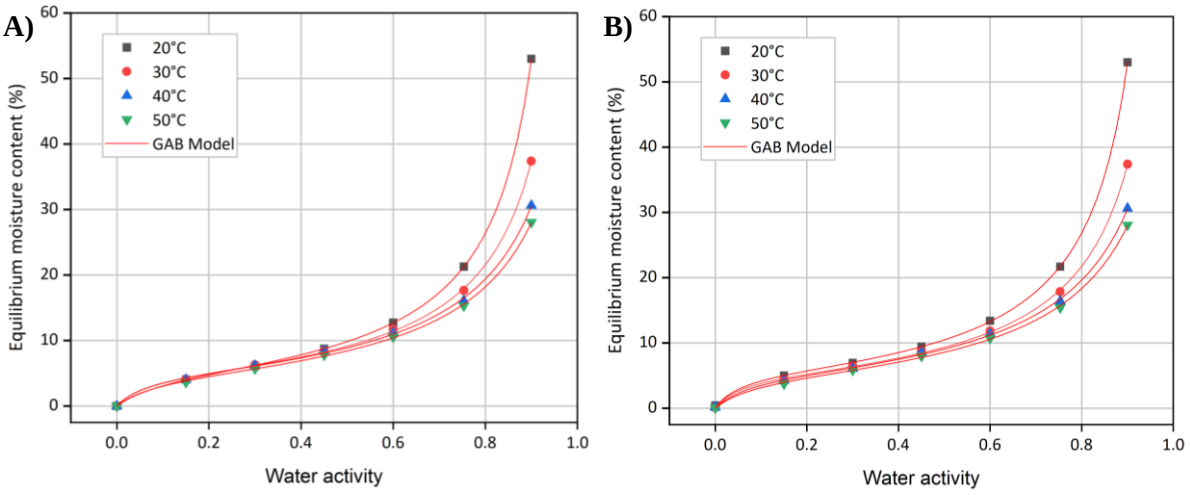

Figure 5. Isotherms of adsorption (A) and desorption (B) of mycelium mat fitted by the GAB model

Table 3: Predicted parameters of GAB model to the experimental data of moisture sorption isotherm of mycelium mat. Standard error of Estimate (RMSE), the coefficient of determination (R^2)

Constants	Desorption data				Adsorption data			
	20°C	30°C	40°C	50°C	20°C	30°C	40°C	50°C
X_m	5.524	5.125	5.266	5.092	5.462	5.059	5.103	5.002
k	0.996	0.960	0.922	0.909	0.998	0.962	0.928	0.916
C	18.939	18.866	14.556	12.485	15.151	15.667	15.709	11.929
R^2	1	0.9999	0.9998	0.9998	1	0.999	0.999	0.999
RMSE	0.228	0.258	0.267	0.233	0.069	0.255	0.305	0.205
SSE	0.208	0.266	0.285	0.218	0.019	0.261	0.372	0.168

4.1.Net isosteric heat of sorption

The net isosteric heat of adsorption and desorption, at constant moisture contents, was calculated by applying the Clausius-Clapeyron equation (Eq. (4)) to the equilibrium isotherm data using the GAB model.

Figure 6 shows the change of the net isosteric heat of sorption as a function of the moisture content. As can be seen, the net isosteric heat of adsorption and desorption presents higher values (9 and 13 kJ.mol^{-1}, respectively) at low moisture sorption content and decreases sharply as the moisture content rises, remaining almost constant (3 kJ.mol^{-1}) above moisture content of

15%. The high net isosteric heat values at low moisture content indicate a strong binding connection of water molecules to the solid due to the presence of a highly active polar site on the surface (monomolecular layer). In addition, this may also be related to the resistance of the movement of water coming from the interior to the surface of the solid. When the moisture content increases, the available active polar sites for water adsorption are diminished, and the strength of the water molecule connection reduces, which conducts in lower value of net isosteric heat of adsorption and desorption. Note that, theoretically, the net isosteric heat tends towards zero at the limit of the hygroscopic domain. However, the derivative in equation 5 is limited here to a moisture content of 28% since four temperatures were considered, resulting in a lack of values at higher water activities, namely above 50°C.

It can also be seen in Figure 6 that the net isosteric heat of sorption values are higher in desorption than in adsorption for mycelium mat at a given moisture content. This means that the conformation, interactions between water molecules and macromolecules of the structure, depends on the history of the product. In fact, the energy demand increase in the desorption process is characterized by the existence of more polar sites on the surface with less mobility of the water molecules to the exit of the material.

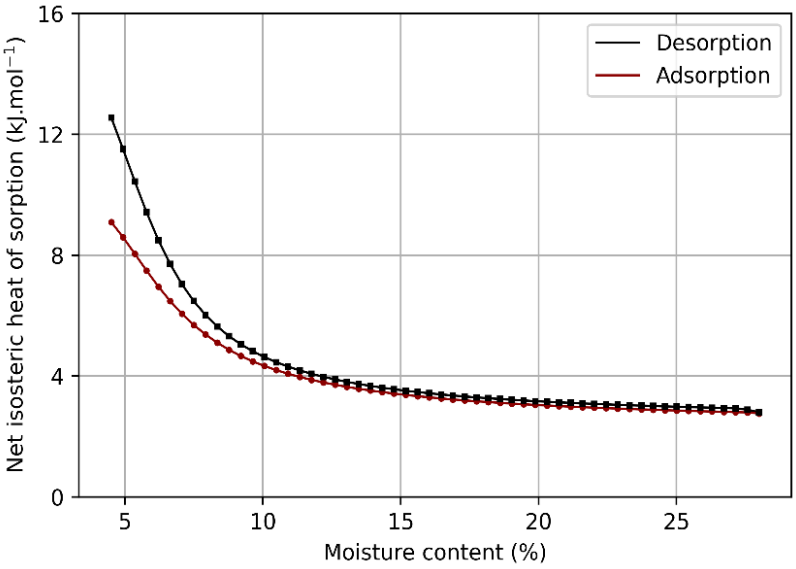

Figure 6. Net isosteric heat of sorption of mycelium mat as a function of equilibrium water content.

4.2.Sorption differential entropy

Figure 7 presents the variation of differential entropy for mycelium mat as a function of equilibrium moisture content. As for the net isosteric heat of sorption, the sorption entropy also

depends on the moisture content. The desorption entropy presents a higher value (25 J/K. mol) at low moisture sorption content and decreases rapidly as the moisture content rises and remains nearly constant (8 J/K. mol) above the moisture content of 15%. A similar trend can also be observed for adsorption entropy. A sharp decrease in adsorption entropy, from 15 to 8 J/K. mol, is observed with increasing moisture content. This could be explained by the decrease in the order of water molecules with an increase in moisture content. It is well known that the sorption entropy is proportional to the number of available sorption sites at specific energy levels. When the moisture content is low, the water molecules can be bound to many available sites. In contrast, when the moisture content increases, the available active sites become occupied and reduced, conducting in a decrease in the sorption entropy. Figure 7 also reveals that the differential entropy of the desorption process presents slightly higher values than that for adsorption at low moisture, which is consistent with the fact that more sorption sites exist in desorption compared to adsorption. Similar behavior has been observed for various materials such as wood [45], argan pulp and leaves [46], and cement-based materials [39].

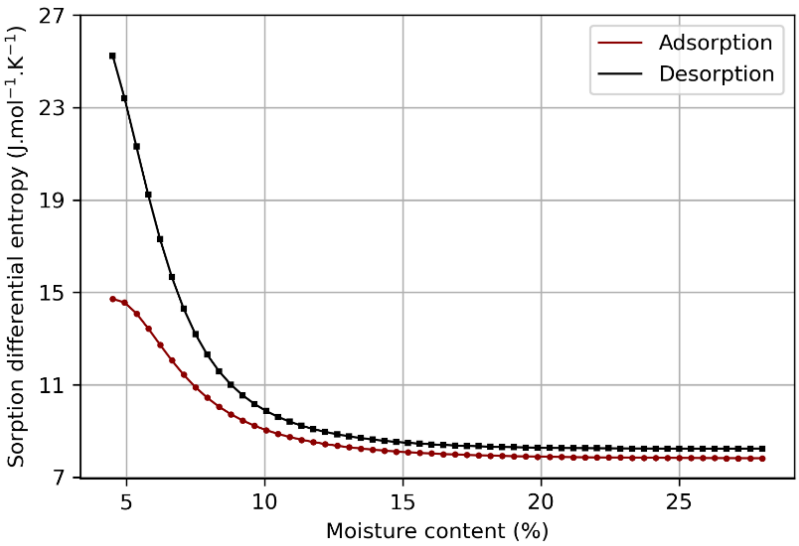

Figure 7: Sorption differential entropy of mycelium mat as a function of equilibrium water content

4.3. Enthalpy-entropy compensation theory

The enthalpy-entropy compensation theory evaluates physical and chemical phenomena such as sorption reactions. Figure 8 presents the net isosteric heat of sorption versus the sorption differential entropy for the mycelium mat. The curves depict a linear relationship with a correlation coefficient of R^2 =0.993 and R^2 =0.990 for adsorption and desorption, respectively. It means that compensation can be employed in the investigated moisture content range. The

harmonic mean temperature (T_{hm}) is found to be equal to 309.15 K, which is significantly lower than the obtained values of T_{β} (Table 4). Since the isokinetic temperature values are higher than the harmonic temperature value ($T_{\beta} > T_{hm}$), the sorption processes can be considered as enthalpy driven. It is similar to the reported by Gabas et al. 2000 for the vapor water adsorption by dried plum skin and pulp. The authors suggested that this indicates the sample microstructure was stable, not undergoing changes during water adsorption.

The free energy ΔG_{β} values at temperature T_{β} indicate the affinity of the mycelium mat for water and if the water sorption process is spontaneous or non-spontaneous. The values ΔG_{β} are negatives (-0.77 and -2.90 kJ/mol for desorption and adsorption, respectively) which means that the sorption processes of mycelium mat are spontaneous. Different authors found similar behavior for different materials, such as wood and starch [30, 45].

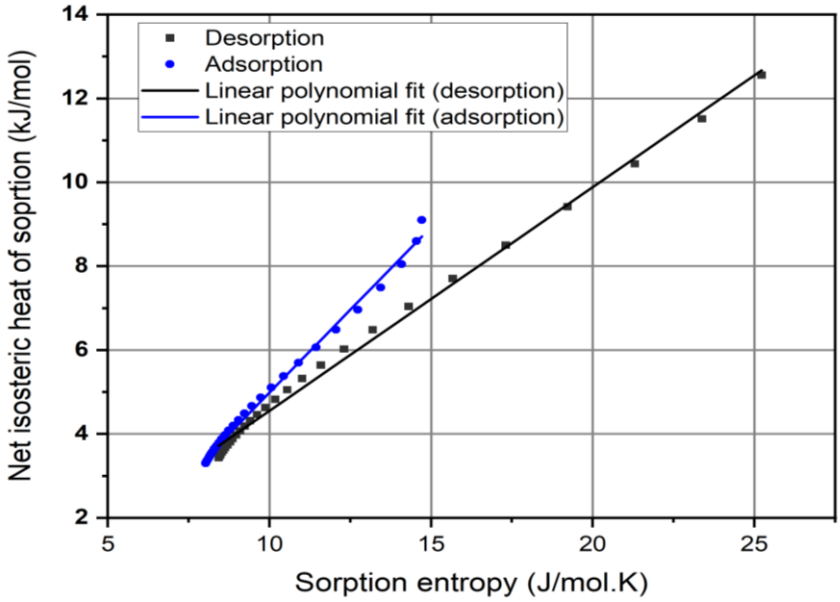

Figure 8: Enthalpy–Entropy relationship effect for water adsorption-desorption processes

Table 4: Enthalpy-entropy theory results.

Sorption isotherms	T_{β} [K]	ΔG_{β} [kJ.mol^{-1}]	R^2
Desorption	533.11	-0.77	0.993
Adsorption	789.08	-2.90	0.990

4.4. Dynamics of moisture transfer

To prepare the inverse analysis, a python script was written to automatically extract the transient periods of all stepwise changes of RH from the Excel file generated by the IGASorp-HT system. The two extreme temperature levels (20°C and 50°C) were analyzed. As an example of raw data, Figure 9 plots the six transient periods measured at 50°C.

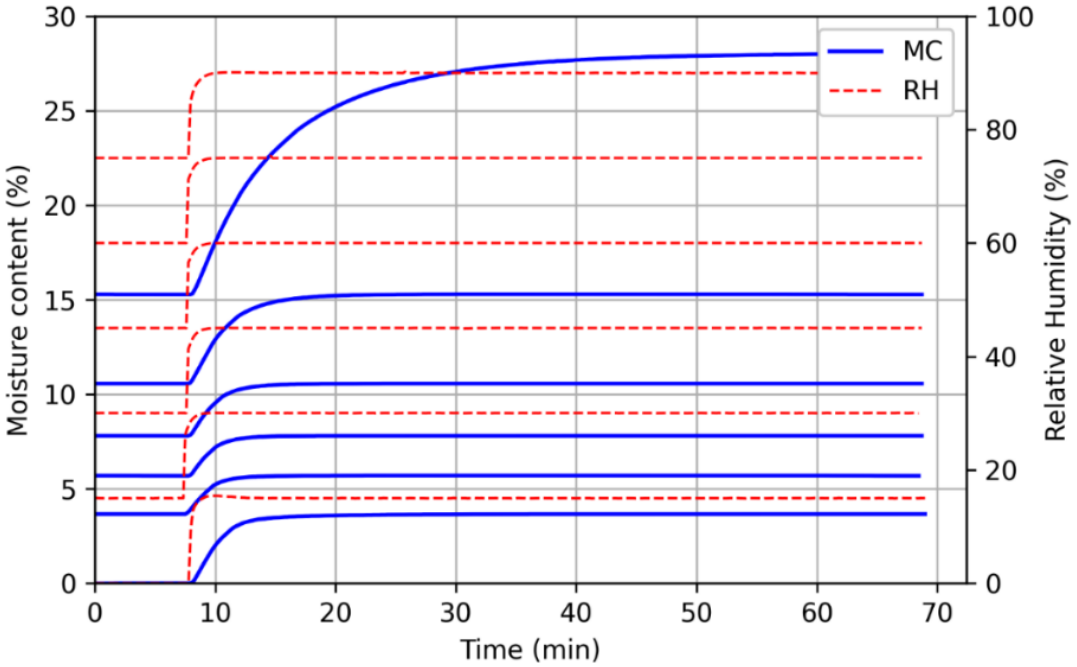

Figure 9:Transient phases extracted from the sorption experiment at 50°C (actual values of RH and MC stored during the sorption test).

The sample used for the sorption test had a thickness of 0.4 mm and a density of 491 kg.m^{-3}. Using a density of 1430 kg.m^{-3} for the mycelium phase [48], the porosity of the sample is equals 66%. Due to the sample thinness, it is not possible to identify the dimensionless diffusivity f from the transient phases of the sorption tests. Instead, the value predicted using the mixture law proposed in [49] for low density fiberboards, porous media with very similar pore morphology, was used. The dimensionless diffusivity obtained for a solid fraction of 0.34 is $f = 0.35$. For better accuracy, the actual RH and temperature values, as recorded by the device versus time, were used in the inverse analysis, instead of the set values.

As examples, Figure 10 depicts the identification results for a set of three RH steps at 50°C (0% - 15%, 45% - 60% and 75% - 90%). The first one (0% - 15%) clearly demonstrates that a "simple" macroscopic formulation of coupled transfer is unable to represent the actual dynamics of moisture uptake. The resistance to mass transfer of the macroscopic model is so rapid that

the moisture content can follow the overshot in RH of the equipment. As expected, this confirms the presence of a dual-scale effect: the sorption dynamics is mainly controlled by the characteristic time of diffusion inside the solid inclusions.

For the step 45% - 60%, the macroscopic prediction remains fast, but the gap with the experiment is slight. This is a subtle effect of the slope of the molar concentration of vapor with temperature, that increases with relative humidity. Due to this, the potential of external coupled transfer reduces when RH increase. This can be observed as the initial gaps of both the molecular concentration and temperature after the sudden change of RH at the beginning of a new RH step. These gaps have been computed and plotted for a better explanation (see the supplementary material). Yet, a dual-scale effect is still required to fit the experimental curve. It is interesting to observe that the microscopic, diffusivity increased: using then value identified for the first step gives a simulated curve much slower that the experimental one.

The last step plotted in Figure 10, 75% - 90%, show a very slow moisture uptake towards equilibrium (more than 30 minutes to approach equilibrium). The model is perfectly able to predict this dynamic, whatever the assumption (macroscopic or dual-scale). Indeed, in this case, the effect of RH on the external potential is even reinforce by the sorption isotherm. This last RH gap of 15% produces a change of moisture content of 12.7% (against 3.6% and 2.7 %, respectively, for the previous steps). For the same exchange surface, and a reduced potential of external coupled transfers, the quantity of water uptake is increased by a factor 3 to 4. This demand further slows down the dynamics. This last step is indeed mostly controlled by the external resistance to transfer. Consequently, the identification of microscopic diffusivity lakes of accuracy. The identification just tells us that this microscopic diffusion must be large enough to avoid the simulated curve to be slower than the experiment.

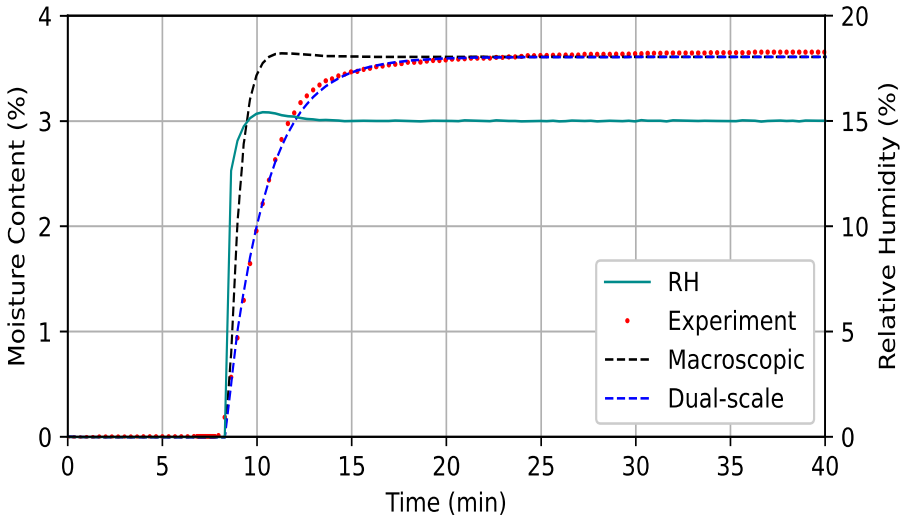

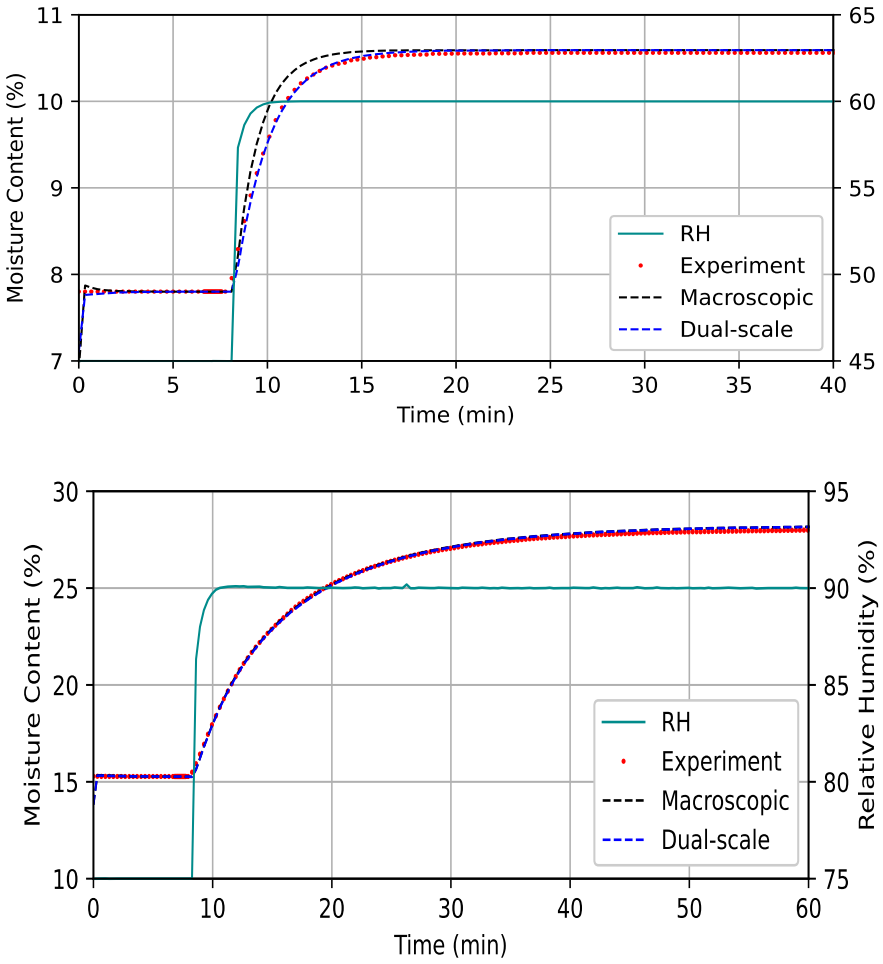

Figure 10: Inverse analysis of sorption tests using a classical and a dual-scale formulations. Examples for the test at 50°C and three different RH steps (from top to bottom: 0% - 15%, 45% - 60% and 75% - 90%).

One final remark: in all the simulations performed at 20°C and 50°C, the internal macroscopic profiles were always almost flat, which confirms that the dynamics of transfers is either controlled by the microscopic scale, or by external exchanges.

Table 5 summarize the dynamics properties of water migration in the fungal materials produced in this work. The thermo- and hydro-activation of diffusivity of bound water (inside inclusions), well-established for materials of biological origin [15, 35], is confirmed here. For example, the values are four times larger at 50°C compared to 20°C. Note that the dimensionless macroscopic diffusivity f is not affected by temperature or moisture content as it accounts for water vapor diffusion in the gaseous phase. As this parameter represent a fraction of vapor diffusivity in air D_v, the effect of temperature and moisture is accounted by the thermo-activation of D_v and

the hydro and thermo-activation of ρ_v through the saturated water vapor pressure and the sorption isotherms, both accounted for in the computational model *TransPore*.

Table 5: Characterization of moisture transfer parameters: microscopic diffusivity in mycelium hyphae, moisture content range and dimensionless macroscopic diffusivity f for each experimental RH step. An average diameter of 20 µm is assumed to determine the microscopic bound water diffusivity.

RH step (%)	20°C		50°C	
	Diffusivity (m^2s^{-1})	X_m range (%)	Diffusivity (m^2s^{-1})	X_m range (%)
0 - 15	$3.2\ 10^{-14}$	0 - 4.7	$1.5.\ 10^{-13}$	0 - 3.9
15 - 30	$3.5.\ 10^{-14}$	4.7 - 6.7	$2.3.\ 10^{-13}$	3.9 - 5.6
30 - 45	$4.2.\ 10^{-14}$	6.7 - 9.2	$3.5.\ 10^{-13}$	5.6 - 7.6
45 - 60	$5.4.\ 10^{-14}$	9.2 - 13.0	$4.3.\ 10^{-13}$	7.6 - 10.4
60 - 75	$1.1.\ 10^{-13}$	13.0 - 21.2	$5.6.\ 10^{-13}$	10.4 - 15.4
75 - 90	$> 1.5\ 10^{-13}$	21.2 - 53.3	$>1.0.\ 10^{-12}$	15.4 - 28.0
Dimensionless diffusivity (macroscopic scale)	$f = 0.35$			

5. Conclusions

In this work, mycelium mat were elaborated by liquid-state fermentation and its relation with water was evaluated in different ways. Their isotherms were measured at 20°C, 30°C, 40°C, and 50°C, showing a sigmoidal-shaped curve form. It reflects a Type II isotherm, which is typical for most hydrophilic materials, aligning closely with properties observed in some cotton- and leather-based materials. Pure mycelium mats are highly hygroscopic and depict a huge condensation phase at high water activity, with an equilibrium moisture content of 53% at 20 °C and 90% RH. As expected, a decreasing adsorption capacity was observed at increasing temperature. Among the eight isotherm models tested, the GAB model is recommended for its theoretical background together with its small residual errors. The net isosteric heat of adsorption and desorption presents higher values (9 and 13 $kJ.mol^{-1}$, respectively) at low moisture sorption content, and decreases asymptotically towards a final value of 3 $kJ.mol^{-1}$. A similar trend was observed with sorption differential entropy: it decreases with increasing moisture content and remains nearly constant (8 J/K. mol) above the moisture content of 15% dry basis. Enthalpy-entropy compensation, or isokinetic theory, was successfully applied to mycelium mat water sorption, suggesting that the process may occur through enthalpy-

controlled mechanisms. The analysis of the transient sorption phases highlights a clear dual-scale effect of moisture migration, in line with its intrinsic morphology. The observed moisture regulation properties of mycelium mats, akin to those in leather, hint at their potential utility in applications where moisture management is essential, thereby offering a sustainable alternative to conventional materials.

6. Notations

The main notations are summarized in Tables 6–8

Table 6

List symbols (Latin letters)

Symbol	Name	Unit
α_w	Water activity	-
D	Diffusion coefficient	$m^2\ s^{-1}$
h_h	Convective heat transfer coefficient	$W.m^{-2}\ K^{-1}$
h_m	Mass transfer coefficient	$m.s^{-1}$
ΔH_{vap}	Vaporization latent heat of pure water	$kJ.mol^{-1}$
T	Temperature	K or °C
υ	General velocity vector	$m.s^{-1}$
Xm	Moisture content (dry basis)	-
k, C	GAB model coefficients	-
f	Dimensionless diffusion factor	-
P	Pressure	Pa
V	Volume	m^3
M	Molar mass	$kg.mol^{-1}$
ΔG_β	Free energy at the temperature Tβ	$J.mol^{-1}$
Q_{st}	Isosteric heat of sorption	$J.mol^{-1}$
q_{st}	Net isosteric heat of sorption	$J.mol^{-1}$
T_β	Isokinetic temperature	K
T_{hm}	Harmonic mean temperature	K
ΔS	Molar differential entropy of sorption	$J.K^{-1}.\ mol^{-1}$
Lv	Latent heat of vaporization	mol^{-1}
R	Universal gas constant	$kJ.mol^{-1}\ K^{-1}$
RH	Relative humidity	%

Table 7

List symbols (Latin letters)

Symbol	Name	Unit
α	Pre-exponential factor	
ε	volume fraction	
λ	Thermal conductivity	$W.m^{-1}:K^{-1}$
φ	Memory function	
ω	Mass fraction	
ρ	Density	$kg.m^{-3}$
τ	Time constant	s
∂	Partial derivative	
∇	Gradient	
$\nabla\cdot$	Divergence	

Table 8

Subscripts

Symbol	Meaning
a	air
b	Bound water
eff	Effective property
eq	Equilibrium
g	Relative to the gaseous phase
v	Water vapour

Acknowledgments

Communauté urbaine du Grand Reims, Département de la Marne, Région Grand Est and European Union (FEDER Champagne-Ardenne 2014-2020) are acknowledged for their financial support to the Chair of Biotechnology of CentraleSupélec and the Centre Européen de Biotechnologie et de Bioéconomie (CEBB).

Author contributions

Brahim Mazian: Conceptualization; Methodology; Validation; Formal analysis; Investigation; Data Curation Management; Writing – Original Draft; Writing - Review & Editing; Visualization.
Hasna Nait M'barek: Methodology; Validation; Formal analysis; Investigation; Writing - Review & Editing.
Giana Almeida: Methodology; Validation; Formal analysis; Investigation; Data Curation Management; Writing - Review & Editing.
Pedro E. D. Augusto: Formal analysis; Writing - Review & Editing.
Patrick Perré: Conceptualization; Methodology; Software; Formal analysis; Investigation; Resources; Data Curation Management; Writing - Review & Editing; Visualization; Supervision; Project administration; Funding acquisition.

Data and code availability

Data, models and formulations used during this study appear in the submitted article.

Supplementary information

Two valuable additions that complement the main body of the manuscript were added in supplementary materials. Supplementary Table 1S presents the predicted parameters of eight fitted models to the experimental data of moisture sorption isotherm of the mycelium mat, providing further insights into the model fitting process. Supplementary Figure S1 visualizes the potential gap of temperature along successive relative humidity (RH) steps, showcasing the molar concentrations of vapor at saturation and the specific RH values used in the sorption test.

Declaration of Competing Interest

The authors declare that they have no known competing financial interests or personal relationships that could have appeared to influence the work reported in this paper.

References

1. Attias N, Danai O, Abitbol T, et al (2020) Mycelium bio-composites in industrial design and architecture: Comparative review and experimental analysis. Journal of Cleaner Production 246:119037. https://doi.org/10.1016/j.jclepro.2019.119037

2. Elsacker E, Vandelook S, Brancart J, et al (2019) Mechanical, physical and chemical characterisation of mycelium-based composites with different types of lignocellulosic substrates. PLoS ONE 14:e0213954. https://doi.org/10.1371/journal.pone.0213954

3. Sun W, Tajvidi M, Hunt CG, et al (2019) Fully Bio-Based Hybrid Composites Made of Wood, Fungal Mycelium and Cellulose Nanofibrils. Sci Rep 9:3766. https://doi.org/10.1038/s41598-019-40442-8

4. Wainwright M (1992) An introduction to fungal biotechnology

5. Jones M, Gandia A, John S, Bismarck A (2021) Leather-like material biofabrication using fungi. Nature Sustainability 4:9–16. https://doi.org/10.1038/s41893-020-00606-1

6. Porter DL, Hotz EC, Uehling JK, Naleway SE (2023) A review of the material and mechanical properties of select Ganoderma fungi structures as a source for bioinspiration. J Mater Sci 58:3401–3420. https://doi.org/10.1007/s10853-023-08214-y

7. Vandelook S, Elsacker E, Van Wylick A, et al (2021) Current state and future prospects of pure mycelium materials. Fungal Biol Biotechnol 8:20. https://doi.org/10.1186/s40694-021-00128-1

8. Wolfe M, Cao H (2022) The Development and Customer Acceptance of Shoes With Soles Made From Mushroom Mycelium Composite. In: Breaking Boundaries. Iowa State University Digital Press

9. Michalenko GO, Hohl HR, Rast D (1976) Chemistry and Architecture of the Mycelial Wall of Agaricus bisporus. Journal of General Microbiology 92:251–262. https://doi.org/10.1099/00221287-92-2-251

10. Islam MR, Tudryn G, Bucinell R, et al (2018) Mechanical behavior of mycelium-based particulate composites. J Mater Sci 53:16371–16382. https://doi.org/10.1007/s10853-018-2797-z

11. Greetham L, McIntyre R, Winiski J, Araldi S (2015) Mycological biopolymers grown in void space tooling

12. Block SS (1960) Developments in the production of mushroom mycelium in submerged liquid culture. Biotechnol Bioeng 2:243–252. https://doi.org/10.1002/jbmte.390020302

13. M'barek HN, Taidi B, Smaoui T, et al (2019) Isolation, screening and identification of ligno-cellulolytic fungi from northern central Morocco. Biotechnol Agron Soc Environ. https://doi.org/10.25518/1780-4507.18182

14. Perré P (2019) Coupled heat and mass transfer in biosourced porous media without local equilibrium: A macroscopic formulation tailored to computational simulation. International Journal of Heat and Mass Transfer 140:717–730. https://doi.org/10.1016/j.ijheatmasstransfer.2019.06.043

15. Perré P, Rémond R, Almeida G (2022) Multiscale analysis of water vapor diffusion in low density fiberboard: Implications as a building material. Construction and Building Materials 329:127047. https://doi.org/10.1016/j.conbuildmat.2022.127047

16. Haneef M, Ceseracciu L, Canale C, et al (2017) Advanced Materials From Fungal Mycelium: Fabrication and Tuning of Physical Properties. Sci Rep 7:41292. https://doi.org/10.1038/srep41292

17. Brunauer S, Emmett PH, Teller E (1938) Adsorption of Gases in Multimolecular Layers. J Am Chem Soc 60:309–319. https://doi.org/10.1021/ja01269a023

18. Langmuir I (1918) THE ADSORPTION OF GASES ON PLANE SURFACES OF GLASS, MICA AND PLATINUM. J Am Chem Soc 40:1361–1403. https://doi.org/10.1021/ja02242a004

19. Van den Berg C, Bruin S (1981) Water activity and its estimation in food systems, L.B. Rockland, G.F. Stewart Water Activity: Influence on Food Quality. Academic Press, New York

20. Chung DS, Pfost HB (1967) Adsorption and Desorption of Water Vapor by Cereal Grains and Their Products Part I: Heat and Free Energy Changes of Adsorption and Desorption. Transactions of the ASAE 10:0549–0551. https://doi.org/10.13031/2013.39726

21. Enderby JA (1955) Water absorption by polymers. Trans Faraday Soc 51:106. https://doi.org/10.1039/tf9555100106

22. Iglesias HA, Chirife J (1976) A MODEL FOR DESCRIBING THE WATER SORPTION BEHAVIOR OF FOODS. J Food Science 41:984–992. https://doi.org/10.1111/j.1365-2621.1976.tb14373.x

23. Oswin CR (1946) The kinetics of package life. III. The isotherm. J Chem Technol Biotechnol 65:419–421. https://doi.org/10.1002/jctb.5000651216

24. Halsey G (1948) Physical Adsorption on Non-Uniform Surfaces. The Journal of Chemical Physics 16:931–937. https://doi.org/10.1063/1.1746689

25. Peleg M (1992) Assessment of a semi-empirical four parameter general model for sigmoid moisture sorption isotherms. Journal of Food Process Engineering 16:21-37. https://doi.org/10.1111/j.1745-4530.1993.tb00160.x

26. Caurie M (2007) A new model equation for predicting safe storage moisture levels for optimum stability of dehydrated foods. International Journal of Food Science & Technology 5:301–307. https://doi.org/10.1111/j.1365-2621.1970.tb01571.x

27. Arslan-Tontul S (2021) Moisture sorption isotherm and thermodynamic analysis of quinoa grains. Heat Mass Transfer 57:543–550. https://doi.org/10.1007/s00231-020-02978-8

28. Monte ML, Moreno ML, Senna J, et al (2018) Moisture sorption isotherms of chitosan-glycerol films: Thermodynamic properties and microstructure. Food Bioscience 22:170–177. https://doi.org/10.1016/j.fbio.2018.02.004

29. Madamba PS, Driscoll RH, Buckle KA (1996) Enthalpy-entropy compensation models for sorption and browning of garlic. Journal of Food Engineering 28:109–119. https://doi.org/10.1016/0260-8774(94)00072-7

30. McMinn WAM, Al-Muhtaseb AH, Magee TRA (2005) Enthalpy–entropy compensation in sorption phenomena of starch materials. Food Research International 38:505–510. https://doi.org/10.1016/j.foodres.2004.11.004

31. Garvín A, Ibarz R, Ibarz A (2017) Kinetic and thermodynamic compensation. A current and practical review for foods. Food Research International 96:132–153. https://doi.org/10.1016/j.foodres.2017.03.004

32. Leffler JE, Grunwald E (2013) Rates and equilibria of organic reactions: as treated by statistical, thermodynamic and extrathermodynamic methods., Courier Corporation. New York

33. Perré P, Pierre F, Casalinho J, Ayouz M (2015) Determination of the Mass Diffusion Coefficient Based on the Relative Humidity Measured at the Back Face of the Sample During Unsteady Regimes. Drying Technology 33:1068–1075. https://doi.org/10.1080/07373937.2014.982253

34. Challansonnex A, Casalinho J, Perré P (2019) Non-Fickian diffusion in biosourced materials: Experimental determination of the memory function using minute samples. Construction and Building Materials 224:560–571. https://doi.org/10.1016/j.conbuildmat.2019.07.013

35. Perré P, Challansonnex A, Colin J (2019) On the importance of heat and mass transfer coupling for the characterization of hygroscopic insulation materials. International Journal of Heat and Mass Transfer 133:968–975. https://doi.org/10.1016/j.ijheatmasstransfer.2018.12.105

36. Zhang W, Chen X, Liu G, et al (2022) Study on the chemical changes of Quercus acuttisima by Ganoderma lucidum cultivation after different years by FTIR analysis. Spectrochimica Acta Part A: Molecular and Biomolecular Spectroscopy 266:120443. https://doi.org/10.1016/j.saa.2021.120443

37. Antinori ME, Contardi M, Suarato G, et al (2021) Advanced mycelium materials as potential self-growing biomedical scaffolds. Sci Rep 11:12630. https://doi.org/10.1038/s41598-021-91572-x

38. Almeida G, Rémond R, Perré P (2018) Hygroscopic behaviour of lignocellulosic materials: Dataset at oscillating relative humidity variations. Journal of Building Engineering 19:320–333. https://doi.org/10.1016/j.jobe.2018.05.005

39. Ben Abdelhamid M, Mihoubi D, Sghaier J, Bellagi A (2016) Water Sorption Isotherms and Thermodynamic Characteristics of Hardened Cement Paste and Mortar. Transp Porous Med 113:283–301. https://doi.org/10.1007/s11242-016-0694-y

40. Fakhfakh R, Mihoubi D, Kechaou N (2018) Moisture sorption isotherms and thermodynamic properties of bovine leather. Heat Mass Transfer 54:1163–1176. https://doi.org/10.1007/s00231-017-2223-0

41. Suppakul P, Chalernsook B, Ratisuthawat B, et al (2013) Empirical modeling of moisture sorption characteristics and mechanical and barrier properties of cassava flour film and their relation to plasticizing–antiplasticizing effects. LWT - Food Science and Technology 50:290–297. https://doi.org/10.1016/j.lwt.2012.05.013

42. Zhang X, Li J, Yu Y, Wang H (2018) Investigating the water vapor sorption behavior of bamboo with two sorption models. J Mater Sci 53:8241–8249. https://doi.org/10.1007/s10853-018-2166-y

43. Bhouri N, Bennasrallah S, Perre P (2012) Influence of geometrical structure on sorption isotherms of Jersey and yarns made of cotton at two temperatures. Microporous and Mesoporous Materials 163:76–84. https://doi.org/10.1016/j.micromeso.2012.07.024

44. Salmén L, Larsson PA (2018) On the origin of sorption hysteresis in cellulosic materials. Carbohydrate Polymers 182:15–20. https://doi.org/10.1016/j.carbpol.2017.11.005

45. Simón C, Esteban LG, de Palacios P, et al (2016) Thermodynamic properties of the water sorption isotherms of wood of limba (Terminalia superba Engl. & Diels), obeche (Triplochiton scleroxylon K. Schum.), radiata pine (Pinus radiata D. Don) and chestnut (Castanea sativa Mill.). Industrial Crops and Products 94:122–131. https://doi.org/10.1016/j.indcrop.2016.08.008

46. Moussaoui H, Kouhila M, Lamsyehe H, et al (2020) Moisture sorption measurements and Thermophysical characterization of the Taraxacum officinale leaves and root. Heat Mass Transfer 56:2065–2077. https://doi.org/10.1007/s00231-020-02838-5

47. Gabas AL, Menegalli FC, Telis-Romero J (2000) Water Sorption Enthalpy-Entropy Compensation Based on Isotherms of Plum Skin and Pulp. J Food Science 65:680–680. https://doi.org/10.1111/j.1365-2621.2000.tb16072.x

48. Islam MR, Tudryn G, Bucinell R, et al (2017) Morphology and mechanics of fungal mycelium. Sci Rep 7:13070. https://doi.org/10.1038/s41598-017-13295-2

49. Louërat M, Ayouz M, Perré P (2018) Heat and moisture diffusion in spruce and wood panels computed from 3-D morphologies using the Lattice Boltzmann method. International Journal of Thermal Sciences 130:471–483. https://doi.org/10.1016/j.ijthermalsci.2018.05.009